GENERAL WAVE MODEL FOR LARGE COASTAL AREAS

UN MODÈLE GÉNÉRAL DE HOULE POUR DES ZONES CÔTIÈRES DE GRANDE EMPRISE

P. AVILEZ-VALENTE, F. VELOSO-GOMES
Faculdade de Engenharia da Universidade do Porto, Portugal
J.S. ANTUNES DO CARMO, F.J. SEABRA-SANTOS
IMAR-Dept Eng. Civil, Universidade de Coimbra, Portugal

ABSTRACT: Two different initial conditions — cold start and Berkhoff's linear solution — are compared, for a two-dimensional depth-integrated shallow water gravity surface wave propagation model, capable of predicting wave shoaling, refraction, reflection, diffraction and breaking. The model is based on a finite element approximation of the time dependent quasi-irrotational Boussinesq equations with improved dispersion properties. The numerical resolution of these equations leads to a very fine discretization and to huge sparse matrices. A cold start leads as well to relative long term simulations, before a stationary situation is reached. To avoid this inconvenience, the use of the linear solution as initial condition is discussed.

RESUME : Nous comparons les solutions données par l'utilisation d'un modèle bidimensionel intégré sur la verticale, capable de prédire la propagation des ondes de surface en eau peu profonde, le gonflement, la réfraction, la réflexion, la diffraction et le déferlement, en utilisant deux conditions initiales différentes: le repos et la solution linéaire donnée par un modèle de Berkhoff. Le modèle est basé sur une approximation par éléments finis des équations quasi-irrotationelles de Boussinesq, ayant des caractéristiques dispersives améliorées. La résolution numérique de ces équations requiert une très fine discrétisation et l'utilisation de très grandes matrices. Une initialisation à partir du repos conduit aussi à de longues simulations. Pour éviter cet inconvénient, nous discutons l'utilisation de la solution linéaire de Berkhoff comme condition initiale.

1. INTRODUCTION

The flow characteristics in coastal and estuarine regions is strongly influenced by phenomena induced by propagating waves, like refraction, diffraction, reflection, wave breaking, bottom friction, and nonlinear wave-wave and wave-current interactions. A good knowledge of these phenomena is of vital importance in the fields of coastal protection, and harbour design and maintenance. A numerical model based on the Berkhoff mild slope equation leads to solutions which, for waves propagating in shallow waters, are far removed from reality. On the other side, the usage of a Boussinesq model, modified for better dispersive behaviour in deeper waters, with a rest solution as the initial condition, always requires long term simulations, for a periodic pattern to be established all over the computational domain. This feature is as important as the domain length is large in the wave propagation direction. It is our aim to present a methodology by which the linear model solution is used as the initial condition for the nonlinear one, allowing for a faster convergence of the numerical procedure with a considerable saving in computing time.

Firstly, in section 2, we describe both models and their numerical implementation, based on the finite element method for space discretization. Secondly, in section 3, a case study is presented for which the proposed methodology of analysis is applied, as well the classic approach — rest solution as the initial condition.

Thirdly, in section 4, the results are analysed in the time- and frequency domains and compared for both approaches. Finally, in section 5, conclusions are drawn on the efficiency of the proposed methodology. A few figures are presented at end.

2. WAVE PROPAGATION MODELS

Two wave models were used in this work: an extended Boussinesq model for the propagation of nonlinear dispersive waves; and an elliptic linear mild-slope model which was used to generate an initial conditon to the Boussinesq one.

2.1. Improved Boussinesq model

Let the relative wave height $\epsilon = aH$ be a measure of the nonlinearity, and let the relative depth $\sigma = \kappa H$ be a measure of the dispersivity. a is a typical wave height, κ is a characteristic wave number and H is the mean water depth. For weakly nonlinear waves, $\epsilon << 1$, with the relative wave height having a value close to the square of the relative depth, $\mathcal{O}(\epsilon) \approx \mathcal{O}(\sigma^2)$ the wave propagation is governed by the Boussinesq equations [6].

Herein we adopted an extended Boussinesq model [1, 2] which takes into account: an uneven bottom; the bottom friction; the breaking waves effects. Improved dispersive characteristics, with a coefficient depending on the local value of σ for the dispersive term, as deduced by Seabra-Santos [12], have also been included. For a quasi-irrotational flow, it reads:

$$\begin{aligned}
&\frac{\partial h}{\partial t} + h\,\nabla\cdot\mathbf{u} + \mathbf{u}\cdot\nabla h = 0\,,\\
&\frac{\partial \mathbf{r}}{\partial t} = -(\mathbf{u}\cdot\nabla)\,\mathbf{u} - g\nabla(h+\xi) - \frac{1}{\rho h}\,\boldsymbol{\tau}_b\,,\\
&\mathbf{r} = \mathbf{u} - \beta\,\nabla^2\mathbf{u}\,,
\end{aligned} \tag{1}$$

where $\beta = \frac{1}{\kappa^2}\left(\frac{\kappa(H-\xi)}{\tanh[\kappa(H-\xi)]} - 1\right)$. $\mathbf{u} = \mathbf{u}(x,y,t) = (u,v)$ is the horizontal depth averaged velocity field, $h = H - \xi + \eta$ is the total depth, $\xi = \xi(x,y)$ is the bottom elevation, and $\eta = \eta(x,y,t)$ is the surface elevation. $\boldsymbol{\tau}_b = (\tau_{b_x}, \tau_{b_y})$ are the bottom stresses, $\mathbf{r} = (r,s)$ is the horizontal surface velocity field and ρ is the water density. For the sake of simplicity, some bottom derivatives are not presented.

2.1.1. Weak formulation

The weak residual formulation for model (1), after discretization in space by means of a finite element method and in time through a two-point finite difference scheme, reads: find $\hat{h}^{t+\Delta t}$ in $\mathcal{V}^0$, and $\hat{\mathbf{u}}^{t+\Delta t}$ and $\hat{\mathbf{r}}^{t+\Delta t}$ in $\mathcal{V}^0 \times \mathcal{V}^0$, that, for all $\hat{w}$ in $\mathcal{V}^0$ and for all $\hat{\mathbf{w}}$ in $\mathcal{V}^0 \times \mathcal{V}^0$, are such that

$$\begin{aligned}
&\int_\Omega \Big[\hat{w}\,\hat{h}^{t+\Delta t} + \Delta t\,\theta\,\hat{w}\,\left(\nabla\cdot\hat{\mathbf{u}}^{t+\theta\Delta t}\right)\hat{h}^{t+\Delta t}\\
&\quad + \Delta t\,\theta\,\hat{w}\,\hat{\mathbf{u}}^{t+\theta\Delta t}\cdot\nabla\hat{h}^{t+\Delta t}\Big]\,\mathrm{d}\Omega =\\
&\int_\Omega \Big[\hat{w}\,\hat{h}^{t} - \Delta t\,(1-\theta)\,\hat{w}\,\left(\nabla\cdot\hat{\mathbf{u}}^{t+\theta\Delta t}\right)\hat{h}^{t}\\
&\quad - \Delta t\,(1-\theta)\,\hat{w}\,\hat{\mathbf{u}}^{t+\theta\Delta t}\cdot\nabla\hat{h}^{t}\Big]\,\mathrm{d}\Omega
\end{aligned} \tag{2}$$

$$\begin{aligned}
&\int_\Omega \hat{\mathbf{w}}\cdot\hat{\mathbf{r}}^{t+\Delta t}\mathrm{d}\Omega\\
&= \int_\Omega \Big\{\hat{\mathbf{w}}\cdot\hat{\mathbf{r}}^{t} - \Delta t\,\hat{\mathbf{w}}\,\left(\hat{\mathbf{u}}^{t+\theta\Delta t}\cdot\nabla\right)\hat{\mathbf{u}}^{t+\theta\Delta t}\\
&\quad - \Delta t\,g\,\hat{\mathbf{w}}\cdot\left[\nabla\left(\hat{h}^{t+\theta\Delta t} + \xi\right)\right]\\
&\quad - \frac{\Delta t}{\rho\,\hat{h}^{t+\theta\Delta t}}\,\hat{\mathbf{w}}\cdot\boldsymbol{\tau}_b^{t+\theta\Delta t}\Big\}\,\mathrm{d}\Omega
\end{aligned} \tag{3}$$

$$\begin{aligned}
&\int_\Omega \Big(\hat{w}\,\hat{u}^{t+\Delta t}\\
&+\beta\,\nabla\hat{w}\cdot\nabla\hat{u}^{t+\Delta t} + \hat{w}\,\nabla\beta\cdot\nabla\hat{u}^{t+\Delta t}\Big)\,\mathrm{d}\Omega\\
&= \int_\Omega \hat{w}\,\hat{r}^{t+\Delta t}\,\mathrm{d}\Omega + \oint \hat{w}\,\beta\,\frac{\partial\hat{u}^{t+\Delta t}}{\partial\mathbf{n}}\,\mathrm{d}\Gamma
\end{aligned} \tag{4}$$

$$\begin{aligned}
&\int_\Omega \Big(\hat{w}\,\hat{v}^{t+\Delta t}\\
&+\beta\,\nabla\hat{w}\cdot\nabla\hat{v}^{t+\Delta t} + \hat{w}\,\nabla\beta\cdot\nabla\hat{v}^{t+\Delta t}\Big)\,\mathrm{d}\Omega\\
&= \int_\Omega \hat{w}\,\hat{s}^{t+\Delta t}\,\mathrm{d}\Omega + \oint \hat{w}\,\beta\,\frac{\partial\hat{v}^{t+\Delta t}}{\partial\mathbf{n}}\,\mathrm{d}\Gamma
\end{aligned} \tag{5}$$

In the above statement, $\mathcal{V}^0$ is the usual space of C^0 bilinear finite element interpolating functions [13], and $X^{t+\theta\Delta t} = \theta X^{t+\Delta t} + (1-\theta)X^t$, with $0.5 \le \theta \le 1$. Equations (2–5) are solved using a predictor-corrector scheme and a direct solver for matrix inversion. Details on the treatment of boundary and dissipative terms, and on the iterative scheme can be found elsewhere [1, 2].

2.2. Mild-slope model

A linear approximation to the sea surface elevation caused by the propagation of a small amplitude time-harmonic wave, $\eta = \mathrm{Re}\,(\tilde{\eta}\, e^{-i\omega t})$, can be obtained as the solution of the extended mild-slope equation [4, 5, 9, 10]:

$$\nabla \cdot (c\, c_g\, \nabla \tilde{\eta}) + \frac{c_g}{c}\omega^2 \tilde{\eta} + i\,\omega W \tilde{\eta} = 0 \quad . \tag{6}$$

where $\tilde{\eta} = \tilde{\eta}(x, y)$ is a complex function including both the amplitude and phase of the surface elevation, c and c_g are Airy's phase and group celerities, respectively, and ω is the wave angular frequency. W is the ratio between the energy dissipation per surface unit area per unit time and the energy per unit area. A linear approximation for the velocity field can be derived as $\mathbf{u} = \mathrm{Re}\left(-i\,\frac{g}{\omega}\,\nabla\eta\, e^{-i\omega t}\right)$.

2.2.1. Weak formulation

The weak residual formulation for model (6), after discretization in space by means of a finite element method, reads: find $\tilde{\eta}$ in $\mathcal{W}^a$ that, for all $\tilde{\varphi}$ in $\mathcal{W}^0$, is such that

$$\int_\Omega \left[c\, c_g\, \nabla\tilde{\varphi} \cdot \nabla\tilde{\eta} - \frac{c_g}{c}\,\omega^2\,\tilde{\varphi}\,\tilde{\eta} - i\,\omega\, W \tilde{\varphi}\tilde{\eta} \right] \mathrm{d}\Omega = \oint c\, c_g\, \tilde{\varphi}\, \frac{\partial \tilde{\eta}}{\partial \mathbf{n}}\, \mathrm{d}\Gamma \,, \tag{7}$$

where $\mathcal{W}^a = \mathcal{V}^0 + i\,\mathcal{V}^0$.

Details on the treatment of boundary and dissipative terms may be found elsewhere [3]. The resulting system of equations is solved by means of the Quasi-Minimum Residual method [8] with ILUT pre-conditioning [11].

3. CASE STUDY

We applied the above referred model to a case study: the propagation and breaking of a 2 m high sinusoidal wave, with a period of 8 s at an undisturbed depth of 10 m, over a varying depth domain, 500 m long by 900 m wide. The bottom is formed by a slope of 2% in the first 450 m and a 50 m long horizontal platform at shore end. A shore parallel breakwater 300 m long by 20 m wide is located at 220 m far from the offshore boundary. A Manning-Strickler coefficient of 0.025 (S.I. units) was adopted for bottom friction. The wave propagates in the positive x-direction. Thanks to the symmetry, only half-domain was considered (cf. fig. 6). A spatial mesh with 12720 4-node bilinear elements and a total of 12984 points was used. The time step was set to $\Delta t = 0.125$ s. Boundary conditions were total reflection at solid walls and symmetry boundary, and 25% energy absorption at shore. At incoming boundary a radiation condition was considered for the reflected wave.

Two runs were performed with two different initial conditions: (A) cold start — $\eta^0 = 0$, $u^0 = 0$, and $v^0 = 0$; (B) linear solution given by model (7).

Numerical gauges were set at 5 different locations (cf. fig. 6), where surface elevation and velocity field cartesian components were registred and analysed. Gauge 1 is affected by shoalling and reflection from the sea wall. Gauge 2 is mainly affected by shoalling. At gauge 3 both effects of diffraction and breaking are evidents while gauge 4 is mainly affect by breaking and wave reflection from the beach. Gauge 5 is important due to its location at once protected and far from the offshore boundary.

4. RESULTS

The time-series for the surface elevation, η, and for the velocity cartesian components, u and v, were compared for (A) and (B), both by visual inspection and through analysis of the time evolution of the their Fourier harmonics at gauges. In all figures, the dotted line stands for simulation (A) while simulation (B) is represented by the continuous line.

4.1. Time-domain analysis

Figures 1–5 represent the gauge registred time-series. The η- and u-series for (A) and (B) closely match each other at gauges 1 and 2. At gauges 3 and 4 the referred series for (B) have a slightly lower amplitude than the corresponding (A) series, with almost no phase error, while at gauge 5 the (B) amplitude is lower and a phase lag is evident. The differences in the v-series are notorious for all gauges but gauge 5, for

which v is null.

4.2. Frequency-domain analysis

The evolution of the harmonic components of the time-series was studied by means of a FFT analysis with a time window of $\Delta T = 16$ s. Since this is twice the period of the incident wave, the odd harmonic components, $E_1 = E_1(t)$, $E_3 = E_3(t)$, ..., for η, and $U_1 = U_1(t)$, $U_3 = U_3(t)$, ..., for u, and $V_1 = V_1(t)$, $V_3 = V_3(t)$, ..., for v, must vanish in time, since they are a consequence of the transient phenomena — we assumed that the generated lower-harmonics (see [7], chap. 7) have neglectable amplitudes. $E_0 = E_0(t)$, $U_0 = U_0(t)$ e $V_0 = V_0(t)$ are the zeroth-order, mean values, for the surface elevation and the velocity components, respectively, in the time interval $[t - \Delta T, t]$. A stationary, periodic, situation is reached when stable amplitudes are attained for the even harmonics and the odd ones have vanished.

The analysis of the graphics (cf. figs. 7–14) show a faster convergence of simulation (B). Even for the v-series, simulation (B) seems to result in less disturbed amplitudes with more stable mean values, V_0, and main harmonics amplitudes, V_2, and quickly fading odd harmonics. The somewhat different behaviour of (A) and (B) at gauges 3 and 4 might be due to their location in the breaking zone. From the harmonic analysis at those two gauges (cf. figs. 9–12) it seems evident that simulation (B) is quickly converging, while (A) still has oscillating odd harmonics. This long transient in (A) is probably due to the large distance the wave propagates from the entrance boundary. Results at gauge 5 (cf. figs. 13 and 14) seem to confirm this reasoning, although the strong oscillations in (B) registred between $t = 50$ s and $t = 75$ s might indicate that some of the main phenomena (namely breaking) are poorly estimated by (B) and that some improvement must be made.

5. CONCLUSIONS

Several different patterns are visible at five gauges. The general feature is the shortning in simulation time necessary for a stationary situation to be reached when Berkhoff's linear solution is used as an initial condition. This advantage is as important as the domain cross-shore length is large, as in most real life cases. The mean values for the variables and the amplitude of their even harmonics have in this case a faster converging behaviour, while the odd harmonics are, since the beginning of the simulation, of a reduced importance. The simulation time for the run of Boussinesq model for this study case could therefore be reduced by about 50%. Some discrepancies exist for those zones where breaking is the prevailing phenomenon (gauges 3 and 4). We expect that an improvement in the breaking model included in the Berkhoff model might overcome this handicap.

6. REFERENCES

[1] Antunes do Carmo J.S., Seabra-Santos F.J. & Barthélemy E. (1993). Surface waves propagation in shallow water: a finite element model. *Int. J. Num. Meth. in Fluids, Vol. 16, 447-459.*

[2] Antunes do Carmo J.S. & Seabra-Santos F.J. (1996). On breaking waves and wave-current interaction in shallow water: a 2DH finite element model. *Int. J. Num. Meth. in Fluids, Vol. 22, 429–444.*

[3] Avilez-Valente P. (1996). Wave spectrum transformation in the Leixões harbour — a study case. *Proc. III Cong. Métodos Numéricos en Ingeniería, Zaragoza, Vol. 2, 1232–1241*, SEMNI, Barcelona, ISBN 84-87867-73-1.

[4] Berkhoff J.C.W. (1972). Computation of combined refraction-diffraction. *Proc. Int. Coastal Eng. Conf., Vancouver, 471–490.*

[5] Booij N. (1981). Gravity waves on water with non-uniform depth and current. *Ph.D. Thesis, Delft University of Technology.*

[6] Boussinesq J. (1872). Théorie des ondes et des remous qui se propagent le long d'un canal rectangulaire horizontal. *J. Math. Pure et Appl. 2, 17, 55–108.*

[7] Dingemans M.W. (1997). *Water Wave Propagation Over Uneven Bottoms, Part 2*, World Scientific, Singapore.

[8] Freund R.W. & Nachtigal N.M. (1994). An implementation of the QMR method based on coupled two-term recurrences. *SIAM J. Sci. Compu., (15)*.

[9] De Girolamo P., Kostense J.K. & Dingemans M.W. (1988). Inclusion of wave breaking in a mild-slope model. *Proc. Int. Conf. Computer Modelling in Ocean Engng., Venice.*

[10] Hurdle D.P., Kostense J.K., & Van den Bosh P. (1988). Mild-slope model for the wave behaviour in and around harbours and coastal structures in areas of variable depth and flow conditions. *Proc. 2nd Int. Symp. Water Modelling and Measurement, Harrogate.*

[11] Saad Y. (1992). ILUT: a dual threshold incomplete LU factorization. *Research Report, Research Report UMSI 92/38, University of Minnesota Supercomputing Institute, Minneapolis.*

[12] Seabra-Santos F.J. (1994). Modified Boussinesq equations for deep and shallow water monochromatic waves. In *Modelling of Coastal and Estuarine Processes, Estudos de Engenharia Civil, Special Issue (6), 163–172*. ISSN 0870-5011.

[13] Zienkiewicz O.C. (1977). *The Finite Element Method*, 3rd Ed., McGraw-Hill, London.

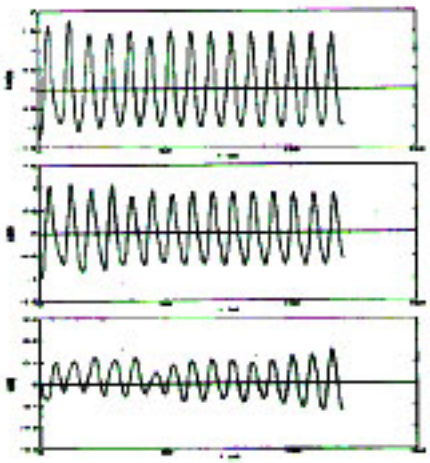

Figure 1: Time series — gauge 1.

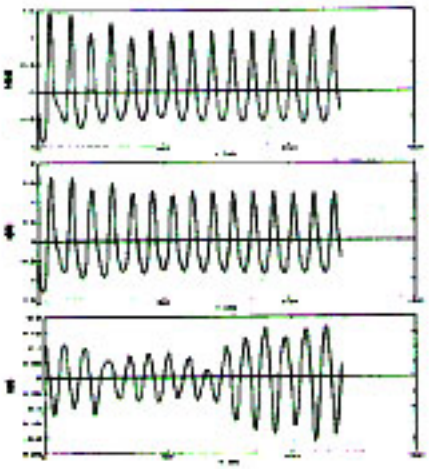

Figure 2: Time series — gauge 2.

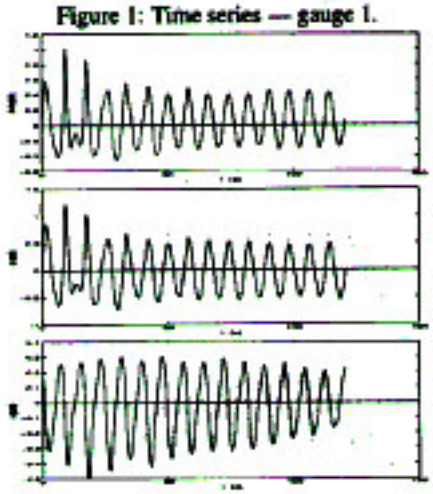

Figure 3: Time series — gauge 3.

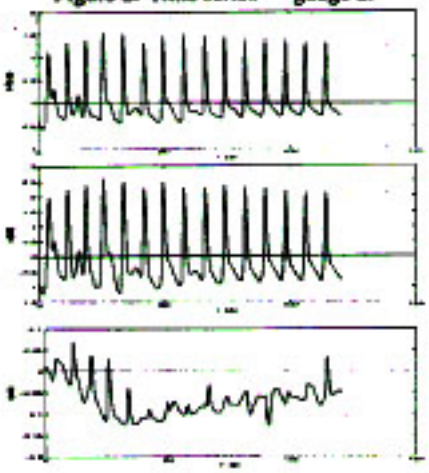

Figure 4: Time series — gauge 4.

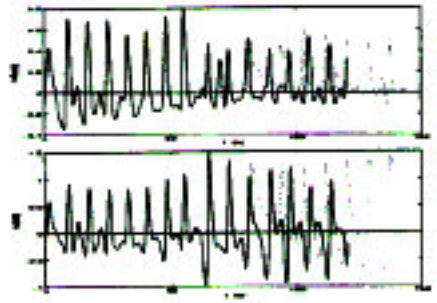

Figure 5: Time series — gauge 5.

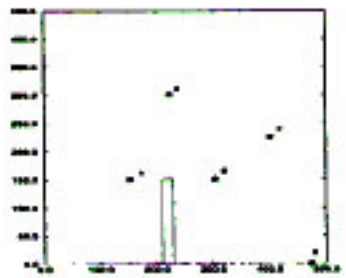

Figure 6: Domain and location of the gauges.

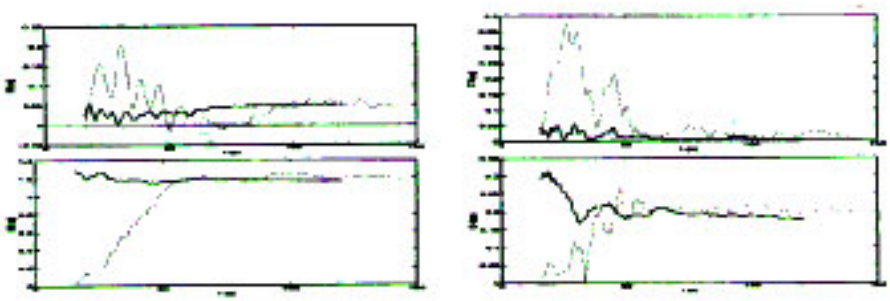

Figure 7: Surface elevation harmonics at gauge 1.

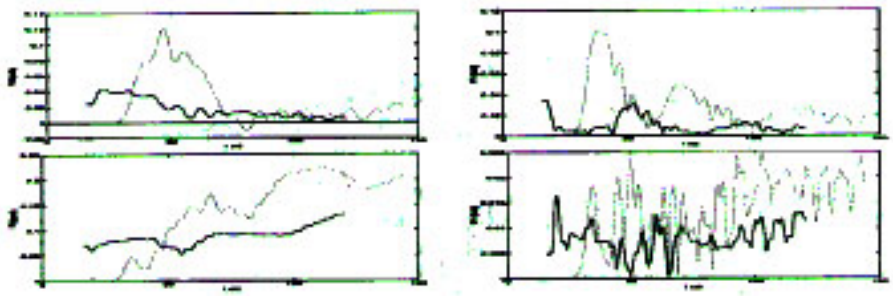

Figure 8: u-velocity harmonics at gauge 1.

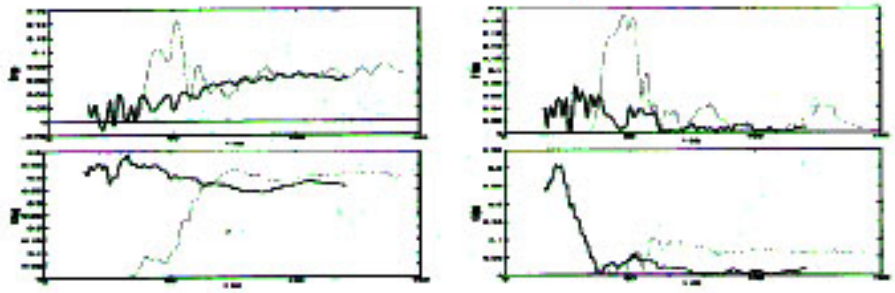

Figure 9: Surface elevation harmonics at gauge 3.

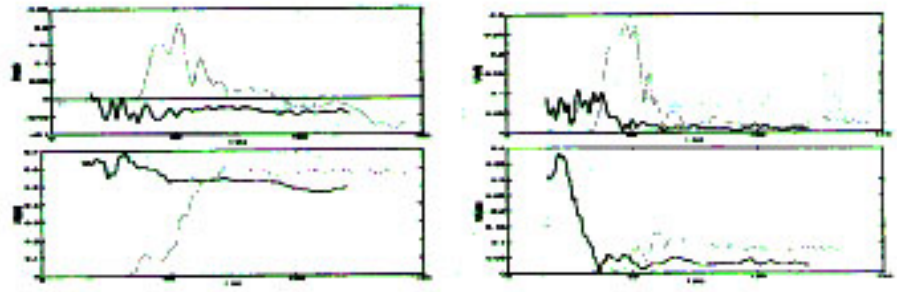

Figure 10: u-velocity harmonics at gauge 3.

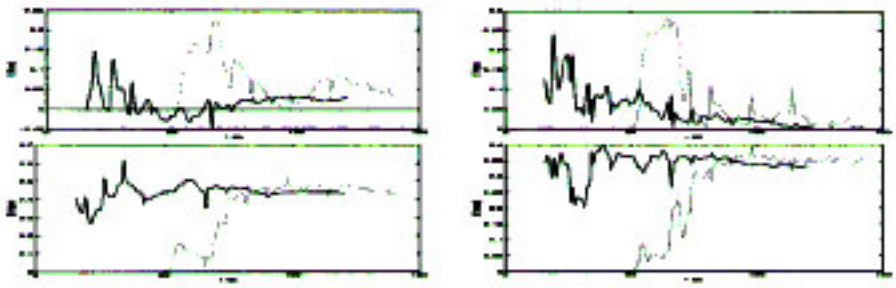

Figure 11: Surface elevation harmonics at gauge 4.

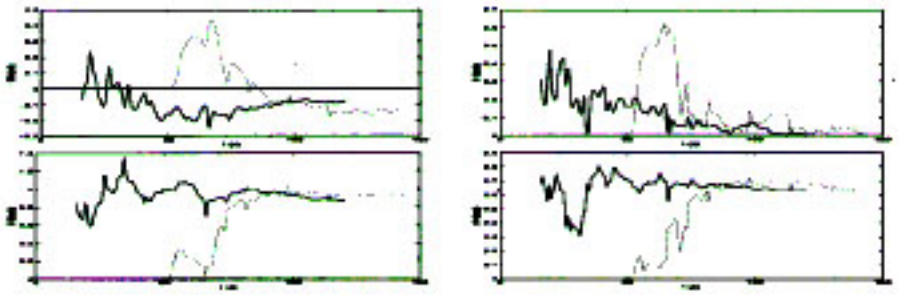

Figure 12: u-velocity harmonics at gauge 4.

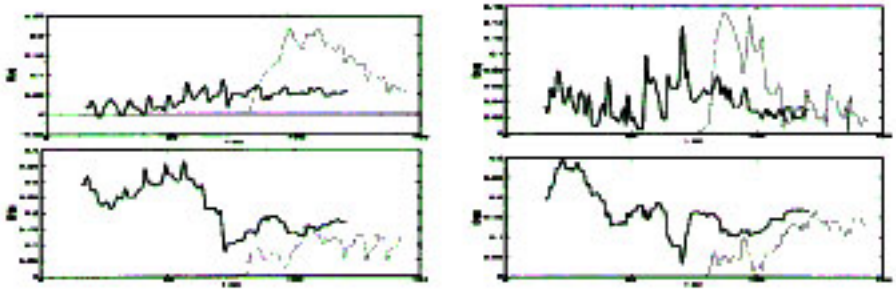

Figure 13: Surface elevation harmonics at gauge 5.

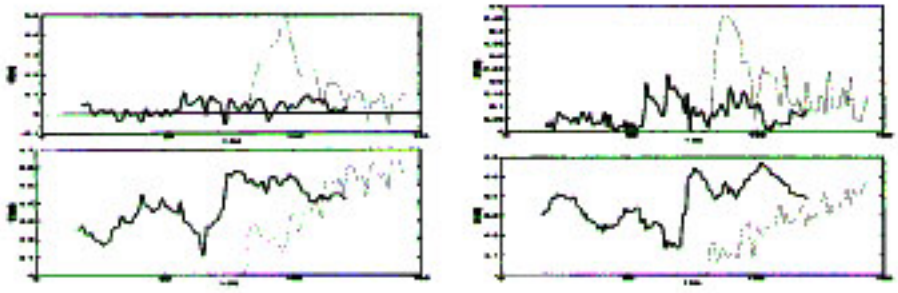

Figure 14: u-velocity harmonics at gauge 5.